doi: 10.82124/CEAS-GNC-2026-002 CEAS-GNC-2026-002

EuroGNC Navigation Guidance Control CEAS Madrid, Spain May 5th-7th uc3m Universidad Carlos III de Madrid AIAA 2026

Linear Time-Varying Control for Accelerating Rockets

Joseph Z. Ben-Asher Professor, Aerspace Engineering, Technion, ITT, Haifa, Israel. yossiba@technion.ac.il

ABSTRACT

The problem of stabilizing and controlling rockets during the boost phase is considered. The rocket may be either fin-stabilized or spin-stabilized in open loop, with additional control surfaces available to enhance stability and disturbance rejection in closed loop. Flight conditions change drastically under forward acceleration. Instead of applying gain scheduling, direct linear time-varying methods, or nonlinear control strategies, the problem is reformulated into a linear time-invariant system by changing the independent variable from time to distance. The control law, designed in the distance domain, is then transformed back to the time domain, resulting in a linear time-varying controller. Nonlinear simulations confirm the effectiveness of the method.

Keywords: Accelerating Rockets, Boost-Phase Stability and Control, Fin Stabilized Rockets, Spin Stabilized Rockets

Nomenclature

α	=	angle-of-attack, $[rad]$
C_D	=	drag coefficient
C_{L_α}	=	derivative of lift force coefficient with respect to α
C_{L_δ}	=	derivative of lift force coefficient with respect to δ
C_{M_0}	=	residual moment coefficient
C_{M_α}	=	derivative of yawing moment coefficient with respect to α
C_{M_δ}	=	derivative of yawing moment coefficient with respect to δ
C_{M_q}	=	derivative of yawing moment coefficient with respect to yaw rate
G_{eff}	=	effective gravity, $[\frac{m}{s^2}]$
I_X	=	moment of inertial around X axis, $[kg \cdot m^2]$
I_Z	=	moment of inertial around Z axis, $[kg \cdot m^2]$
R_m	=	linear thrust misalignment, [m]
S	=	reference area, $[m^2]$
S_b	=	burnout downrange distance, end of acceleration phase, $[m]$
S_g	=	Gyroscopic Stability Factor
T	=	thrust, $[N]$
V	=	velocity, $[\frac{m}{s}]$
$\bar{I}_{sp}$	=	average specific impulse, $[s]$
$\bar{\rho}$	=	average air density in atmosphere, $[\frac{kg}{m^3}]$
Θ_{Z0}	=	nominal elevation angle $[rad]$
β_m	=	angular thrust misalignment, $[rad]$

δ = aerodynamic control surface deflection
δ_0 = residual aerodynamic control surface deflection
γ = azimuth angle, $[rad]$
ρ = air density in atmosphere, $[\frac{kg}{m^3}]$
σ = rocket's wavelength, $[m]$
θ = yaw angle, $[rad]$
d = reference length, $[m]$
g = gravitational acceleration, $[\frac{m}{s^2}]$
l_p = launcher length, $[m]$
m = mean mass, $[kg]$
m_0 = rocket's initial mass, $[kg]$
m_p = rocket's propulsion mass, $[kg]$
p = roll rate $[\frac{1}{sec}]$
s = distance variable, $[m]$
t = time, [s]
t_b = burnout time, end of acceleration phase, $[s]$
w = side-wind velocity normal to the velocity vector $[\frac{m}{s}]$
x = state vector

1 Introduction

Controlling a missile's trajectory during its boost phase is considered a significant and demanding endeavor. During this phase, the missile encounters a broad spectrum of flight conditions due to abrupt changes in its speed. The standard practice of control design is as follows [1][2][3]: Initially, the set of trim points is identified, followed by the design of a set of linear controllers to attain the desired performance at each operational state. Subsequently, the gain is scheduled for each operational point. Finally, the controller's performance is evaluated. This scheme relies on the implicit assumption of time-scale separation. However, this assumption becomes less tenable during periods of high acceleration. Typically, increased axial acceleration enhances the lateral stability of the missile. Consequently, the gain and phase margins obtained from linear analysis tend to be overly conservative.

Recent efforts have been made to design an explicit LTV control for boosting rockets. This typically means: (i) build an LTV model by linearizing the nonlinear launcher dynamics along the ascent trajectory, and (ii) synthesize/assess controllers *directly* on that finite-horizon LTV model rather than using frozen-time LTI grids. Ref. [4] presents a mixed-sensitivity LTV synthesis tailored to pitch attitude control of a flexible launcher, while Ref. [5] provides a rigorous finite-horizon robustness framework that bounds performance under uncertainties during ascent. Addressing the significant nonlinearity of the boost phase may necessitate developing a nonlinear controllers. Various approaches have been proposed toward this goal (e.g., [6][7][8][9]).

The approach outlined in this paper is different. It is widely known that transitioning the independent variable from time to distance, under several simplifying assumptions, results in a linear time-invariant system. The proposition here is to design the controller for this formulation using established linear methods and subsequently convert it back to the time domain. This yields a single linear time-varying controller for the entire phase.

This approach can be applied to fin stabilized rocket, as well as to spin stabilized rocket under simplified assumptions. .

The subsequent sections of the article are structured as follows: Section 2 deals with fin stabilized rocket. Section 2.1 introduces the missile models, both full and approximate, that are being examined. In Section 2.2, two types of missile autopilots are formulated based on PD and PID controllers. Section 2.3 offers numerical simulations to demonstrate the performance of the proposed controller on the full and the

approximate models. Various factors which affect the trajectory of rockets during the acceleration phase, such as tip-off rates, thrust misalignment, gusts and side-wind are tested. Section 3 follows similar steps as Section 2 for a spin stabilized rocket. Lastly, Section 4 provides the concluding remarks for the article.

2 Fin Stabilized Rocket

2.1 Modelling

The acceleration phase of the rocket's trajectory can be approximately treated as a constant acceleration motion. Since it is the first phase of the trajectory, it's outcome affects the remaining trajectory and eventually the ground impact point. For simplicity, this section is focused on the *horizontal* plane but the extension to the longitudinal plane is quite straightforward. The aeroballistic frame of reference, denoted by the letter B, is attached to the accelerating rocket (Figure 1). The origin is located at the rocket's center of mass. X_B axis is directed along the rocket's body towards its tip; the Y_B axis lies in the horizontal plane and is pointing to the right; and Z_B axis completes a right-handed system. An initial aeroballistic frame, B_0, is defined as the rocket's aeroballistic frame at the launching position. This system (B_0) does not travel with the rocket and is fixed at the launching point.

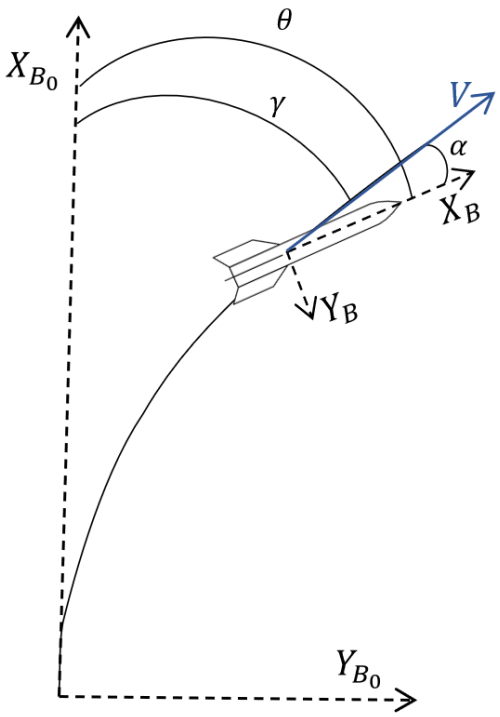

Fig. 1 Rocket's trajectory in the lateral plane with respect to the initial aeroballistic frame

The equations of motion are as follows (for a full derivation see [10] pp.85-93) [1]:

$$\frac{dV}{dt} = \frac{T}{m}\cos(\alpha+\beta_m) - g\sin\Theta_{Z0} - \frac{\rho S C_d}{2m}V^2 \tag{1}$$

$$\frac{d\gamma}{dt} = \frac{T}{mV}\sin(\alpha+\beta_m) + \frac{\rho S C_{L_\alpha}\left(\alpha+\frac{w}{V}\right)}{2m}V + \frac{\rho S C_{L_\delta}(\delta+\delta_0)}{2m}V \tag{2}$$

[1]During burning, the ***non − constant*** gravity terms are negligible compared to the other forces. This greatly simplifies the analysis without causing any significant discrepancies between theoretical predictions and experimental results.

$$\frac{d^2\theta}{dt^2} = \frac{C^*_{M_\alpha}}{d^2}\left(\alpha + \frac{w}{V}\right)V^2 + \frac{C^*_{M_\delta}}{d^2}(\delta + \delta_0)V^2 + \frac{C^*_{M_0}}{d^2}V^2 + \frac{C^*_{M_q}}{2d}\frac{d\theta}{dt}V - \frac{TR_m}{I_Z} \tag{3}$$

$$\theta = \gamma + \alpha \tag{4}$$

where

$$C^*_{M_i} = \frac{\rho S d^3}{2I_Z}C_{M_i} \tag{5}$$

Note that the positive direction of the angles in Figure 1 is clockwise. Also note that in the ***vertical*** plane the second equation has an additional term on the right hand side: $\frac{gcos(\Theta_{Z0})}{V}$.

Following [10], we employ the following assumptions (and the resulting modeling):

1) The angle α is small.
2) The velocity along the acceleration route is linear and can be approximated as: $V = G_{eff}t$.
3) The thrust per unit mass, $\frac{T}{m} = G_{eff}$, is constant. The combined effect of drag and gravity on speed is negligible.
4) There are no disturbances other than side-wind w. Thus : $\beta_m = 0, R_m = 0, \delta_o = 0$.
5) There is no residual moment: $C_{M_0} = 0$.
6) The lift is negligible with respect to the thrust normal components: $C_{L_\alpha} \to 0$, $C_{L_\delta} \to 0$.
7) The aerodynamic damping moment is negligible: $C_{M_q} \to 0$.

Remarks:

1) The first assumption is based on experience. Even for relatively high side-wind the side angle of attack is kept small (see examples below).
2) The second and third assumptions are met in most realistic cases.
3) The fourth and fifth assumptions assume a carefully designed missile; the effects of imperfections will be tested below.
4) The last two assumptions, that is neglecting C_{L_α}, C_{M_q}, and C_{L_δ} , are conservative, in the sense that the first two terms contribute to stability, whereas the last one is typically small.

Define (assuming a statically stable rocket):

$$\sigma \triangleq \frac{2\pi d}{\sqrt{-C^*_{M_\alpha}}} \tag{6}$$

$$t_\sigma \triangleq \sqrt{\frac{2\sigma}{G_{eff}}} \tag{7}$$

$$\xi = \frac{t}{t_\sigma} \tag{8}$$

$$V_\sigma = G_{eff}t_\sigma \tag{9}$$

$$\eta = -\frac{C_{M_\delta}}{C_{M_\alpha}} \tag{10}$$

The derivative with respect to the non-dimensional time ξ will be denoted by:

$$(\quad)' = \frac{d}{d\xi}(\quad) \tag{11}$$

The following linear equations are obtained (see [10] pp.100-102 for the complete derivation):

$$\begin{cases} \xi\gamma' - \alpha & = 0 \\ \theta'' + 16\pi^2\xi^2\left(\alpha + \frac{w}{V}\right) & = 16\pi^2\xi^2\eta\delta \\ \theta & = \gamma + \alpha \end{cases} \tag{12}$$

Notice that by now we are just using a normalized time rather than the elapsed time as our independent variable and we apply our assumptions to the model. A short explanation to the resulting equations is as follows: the first equation is the side acceleration resulting from the thrust component which is proportional to α (the normalized time multiplying the path angle rate results from the velocity which is linear with time). We neglect the aerodynamic side forces, assuming the the thrust is significantly larger. This is why α (the kinematic angle of attack) is of utmost importance, rather than the aerodynamic angle of attack. The post-ballistic miss will largely depend on how well we can keep this angle small. The second equation is for the rigid-body angular acceleration, considering only the aerodynamic moment due to $C^*_{M_\alpha}$ and the aerodynamic moment due to $C^*_{M_\delta}$. The third equation comes from geometry.
Thus

$$\gamma' = \frac{\alpha}{\xi} \quad \Rightarrow \gamma'' = \frac{\alpha'}{\xi} - \frac{\alpha}{\xi^2} \tag{13}$$

$$\theta'' = \gamma'' + \alpha'' = \alpha'' + \frac{\alpha'}{\xi} - \frac{\alpha}{\xi^2} \tag{14}$$

From the second equation in (12), we get

$$\alpha'' + \frac{\alpha'}{\xi} + \left(16\pi^2\xi^2 - \frac{1}{\xi^2}\right)\alpha + \left(16\pi^2\xi^2\right)\frac{w}{V} = \left(16\pi^2\xi^2\eta\right)\delta \tag{15}$$

Using new dependent variables:

$$\omega \equiv \alpha \cdot \xi \Leftrightarrow \alpha = \frac{\omega}{\xi} \quad ; \quad \alpha' = \frac{\omega'}{\xi} - \frac{\omega}{\xi^2} \quad ; \quad \alpha'' = \frac{\omega''}{\xi} - \frac{2\omega'}{\xi^2} + \frac{2\omega}{\xi^3} \tag{16}$$

and

$$\omega_\delta \equiv \delta \cdot \xi \tag{17}$$

Hence,

$$\omega'' - \frac{\omega'}{\xi} + 16\pi^2\xi^2(\omega + \xi\frac{w}{V}) = 16\pi^2\xi^2\eta(\omega_\delta) \tag{18}$$

Finally, let the distance variable $s = \sigma\xi^2$ be a new independent variable. Note that under our assumption s is the actual distance traveled in meters! This is the most important transformation of the present approach, since when distance is used, we get an LTI system :

$$\omega' = \frac{d\omega}{d\xi} = \frac{d\omega}{ds}\frac{ds}{d\xi} = 2\sigma\xi\frac{d\omega}{ds} \tag{19}$$

$$\omega'' = \frac{d^2\omega}{d\xi^2} = 2\sigma\frac{d\omega}{ds} + 2\sigma\xi\frac{d}{d\xi}\left(\frac{d\omega}{ds}\right) = 2\sigma\frac{d\omega}{ds} + 2\sigma\xi\frac{ds}{d\xi}\frac{d}{ds}\left(\frac{d\omega}{ds}\right) = 2\sigma\frac{d\omega}{ds} + (2\sigma\xi)^2\frac{d^2\omega}{ds^2} \tag{20}$$

Substituting in (18), we get

$$\frac{d^2\omega}{ds^2} + \left(\frac{2\pi}{\sigma}\right)^2 \omega + \left(\frac{2\pi}{\sigma}\right)^2 \frac{w}{V_\sigma} = \left(\frac{2\pi}{\sigma}\right)^2 \eta\omega_\delta \tag{21}$$

Note that we have used the connection $V_\sigma = \frac{V}{\xi}$.
Remarks:

1) The harmonic oscillator equation indicates that, in the absence of wind, the angle of attack oscillates with a natural spatial wavelength σ, while its amplitude decreases inversely with time.
2) An identical model was used in Ref. [11] to examine the impact of side wind on uncontrolled rockets. Here, we propose using it for synthesis purposes as well.

2.2 Control Design

The state-space representation of the last equation may be written as:

$$\begin{aligned} \frac{d}{ds}x &= \underbrace{\begin{bmatrix} 0 & 1 \\ -\left(\frac{2\pi}{\sigma}\right)^2 & 0 \end{bmatrix}}_{A} x + \underbrace{\begin{bmatrix} 0 \\ -\left(\frac{2\pi}{\sigma}\right)^2 \end{bmatrix}}_{b} \underbrace{\frac{w}{V_\sigma}}_{d} + \underbrace{\begin{bmatrix} 0 \\ \left(\frac{2\pi}{\sigma}\right)^2 \end{bmatrix}}_{b} \underbrace{\eta\omega_\delta}_{u} \\ x &= \begin{bmatrix} \omega \\ \frac{d}{ds}\omega \end{bmatrix} \end{aligned} \tag{22}$$

The first design will be a PD controller based e.g. on pole placement. It is assumed that the Inertial Navigation System (INS) can provide measurements for the *kinematic* angle-of-attack α and its time derivative. This is a reasonable assumption in modern missiles.
We then obtain

$$\omega_\delta = k_1\omega + k_2\frac{d\omega}{ds} \tag{23}$$

Since $\omega = \alpha\xi$, we get

$$\frac{d\omega}{ds} = \frac{d\alpha}{ds}\xi + \alpha\frac{d\xi}{ds} \tag{24}$$

$$\omega_\delta = k_1\alpha\xi(s) + k_2\frac{\alpha}{2\sigma\xi(s)} + k_2\frac{d\alpha}{ds}\xi(s) \tag{25}$$

$$\delta(s) = \frac{\omega_\delta}{\xi(s)} = k_1\alpha + k_2\frac{\alpha}{2s} + k_2\frac{d\alpha}{ds} \tag{26}$$

Note that s in (26) is *not* the Laplace transform operator. In time domain, we obtain

$$\delta(t) = (k_1 + k_2\frac{t_\sigma^2}{2\sigma t^2})\alpha + k_2\frac{t_\sigma^2}{2\sigma t}\frac{d\alpha}{dt} \tag{27}$$

In designing the control for (22) we may decide to include an integrator (PID controller), thus

$$\omega_\delta = k_1\omega + k_2\frac{d\omega}{ds} + k_3\int \omega ds \tag{28}$$

Accordingly,

$$\delta(s) = \frac{\omega_\delta}{\xi(s)} = k_1\alpha + k_2\frac{\alpha}{2s} + k_2\frac{d\alpha}{ds} + k_3\frac{1}{\xi(s)}\int \alpha\xi(s)ds \tag{29}$$

In time domain the control becomes

$$\delta(t) = (k_1 + k_2\frac{t_\sigma^2}{2\sigma t^2})\alpha + k_2\frac{t_\sigma^2}{2\sigma t}\frac{d\alpha}{dt} + k_3\frac{2\sigma}{tt_\sigma^2}\int \alpha t^2 dt \tag{30}$$

Remark:
The solution starts from the time of leaving the barrel, thus it is not singular at t_0.

2.3 Representative Example

We consider a hypothetical rocket with parameters outlined in Table 1. Certain parameters, like the initial angular rate induced by the launcher (tip-off), will be adjusted later to assess the efficacy of the rocket's closed-loop control.

	Value	Units		Value	Units
l_p	4	$[m]$	t_b	1.26	$[s]$
m_0	97.4	$[kg]$	S_b	614.6	$[m]$
m_p	33.9	$[kg]$	γ_0, θ_0	0	$[^o]$
$\bar{I}_{sp}$	250	$[s]$	$\dot{\theta}_0$	0	$[\frac{rad}{s}]$
d	0.16	$[m]$	θ_{z_0}	53	$[^o]$
I_Z	68.2	$[kg \cdot m^2]$	C_D	0.4	
β_m	0	$[rad]$	C_{M_α}	-27.5	
R_m	0	$[m]$	$C^*_{M_\alpha}$	$-2 \cdot 10^-5$	
G_{eff}	778.3	$[\frac{m}{s^2}]$	$C^*_{M_\delta}$	$2 \cdot 10^-5$	
$\bar{\rho}$	1.225	$[\frac{kg}{m^3}]$	C_{L_α}	7	
S	0.02	$[m^2]$	C_{L_δ}	-1.5	
σ	223.5	$[m]$	C_{M_q}	-800	

Table 1 Parameters of simulated rocket

The speed profile of the rocket is presented in Figure 2. For this rocket the characteristic wave length is $\sigma = 223.5[m]$, and the corresponding time and speed are $t_\sigma = 0.76[sec]$ and $V_\sigma = 589[m/sec]$.
The state equation (22) becomes:

$$\frac{d}{ds}x = \underbrace{\begin{bmatrix} 0 & 1 \\ -0.00079 & 0 \end{bmatrix}}_{A} x + \underbrace{\begin{bmatrix} 0 \\ -0.00079 \end{bmatrix}}_{b}\underbrace{\frac{w}{589}}_{d} + \underbrace{\begin{bmatrix} 0 \\ -0.00079 \end{bmatrix}}_{b}\underbrace{\omega_\delta}_{u} \tag{31}$$

In our PD design, we select $k_1 = 0.0127$ and $k_2 = 50.6329$, positioning the closed-loop poles at $-0.02 + 0.02i$ and $-0.02 - 0.02i$. To incorporate the PID controller, we introduce $k_3 = 0.01$.
Figures 3 and 4 show a comparison between PD and PID controls by the *full* 3-degree-of-freedom (DOF) model in response to a 0.25-second gust and a constant wind, both of 50 m/sec. In these, and the following runs, δ was limited to 30 deg. We observe the distinct characteristics of the controllers. PID exhibits more oscillations under gust, but achieves zero steady-state error under constant wind. This cannot be

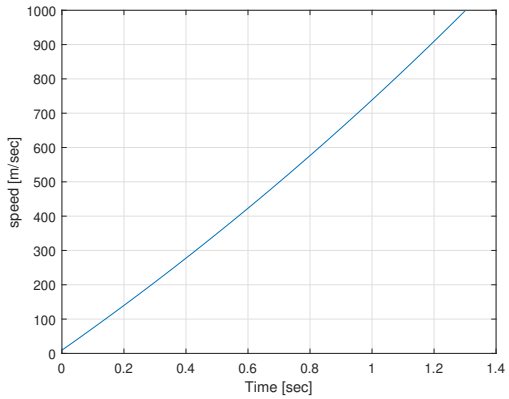

Fig. 2 speed profile

achieved by PD control, as a non-zero trim control is required to counteract the wind moment. Moreover, from (22), we obtain that for PD control the steady-state solution under a constant wind disturbance is reached when

$$\omega \;\rightarrow\; -\frac{d}{1+\eta k_1},$$

which, in our numerical case, yields $\omega \approx -d$ and $\omega_\delta \approx 0$ in steady state.

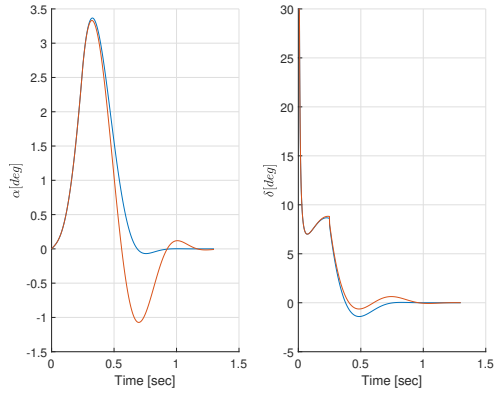

Fig. 3 1^{st} scenario, gust response red PID blue- PD

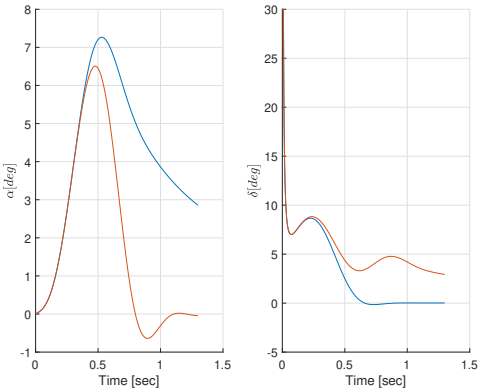

Fig. 4 2^{nd} scenario, constant side-wind red PID blue- PD

Next, we will examine two common disturbances: tip-off rate and thrust misalignment. Figure 5 illustrates the response of the *full* model to a 0.5 [rad/sec] tip-off rate for both controllers.

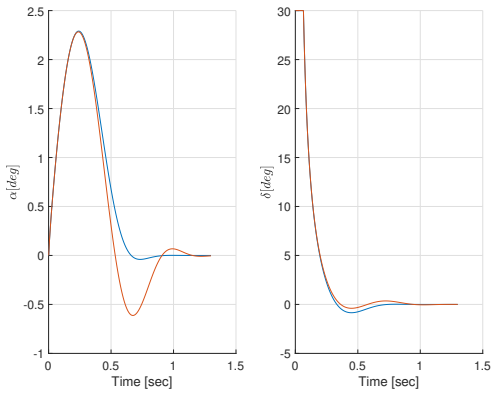

Fig. 5 3^{rd} **scenario, initial tip-off red- PID blue - PD**

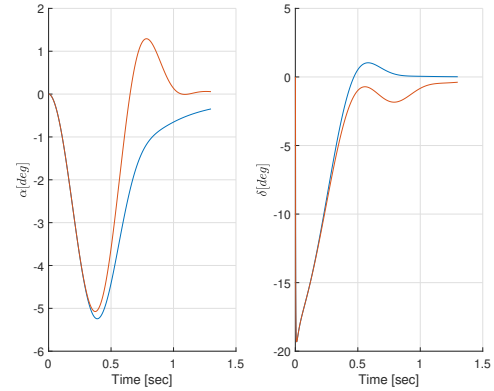

Fig. 6 4^{th} **scenario, thrust misalignment red- PID blue- PD**

Figure 6 depicts the response of the *full* model to a 5 [mm] thrust misalignment for both controllers. Once again, the PID controller shows increased oscillations but ultimately achieves zero steady-state error. In contrast, the PD controller retains a steady-state error, since a non-zero trim input is necessary to balance the thrust moment. Similar arguments as for the constant wind disturbance yields $\omega_\delta \approx 0$ in steady state for the PD controller.

3 Spin Stabilized Rocket

3.1 Modeling

We continue with the same set of assumptions as in the previous section for the fin-stabilized rocket. Additionally, we assume that the Gyroscopic Stability Factor S_g is *constant* throughout the boost phase. Let p be the roll rate around the x axis, then S_g is defined as follows:

$$S_g = \frac{p^2 I_X^2}{2 I_Z V^2 \rho S d C_{M_\alpha}}, \tag{32}$$

Thus, we assume that p (like V) is linear over time. As noted in [10] (p. 317) :
"Experimental tests show that the equations used in this section describe the motion during burning of ground-fired spin-stabilized rockets to within the limits of experimental error, and hence that the solutions given here may be used in predicting the motion of a rocket. The most convincing specific tests were those used in checking the theoretically predicted deflections due to wind and to misalignment, the

experimental results agreeing with the theory to within the experimental error. Perhaps the best check of all on the theory is the fact that it was used throughout an extensive reduction of experimental data for the construction of range tables, and no inconsistencies between theory and experiment were found. "

Note that for open-loop stability, we require $S_g > 1$. To further simplify the notation we assume a vertical launch (no gravity terms in the normal equation). All angles are now complex numbers, i.e. $\alpha = \alpha_Z + i\alpha_Y$; $\theta = \theta_Z + i\theta_Y$; $\gamma = \gamma_Z + i\gamma_Y$. Moreover, the control surfaces are given in an aeroballistic frame: $\delta = \delta_Z + i\delta_Y$. The equations of motion, neglecting gravity and with zero wind, become (for a full derivation, see [10] pp.313-400) :

$$\frac{d\gamma}{dt} - \frac{G_{eff}}{V}\alpha = 0 \tag{33}$$

$$\frac{d^2\theta}{dt^2} - i\frac{I_x p}{I_Z}\frac{d\theta}{dt} - \frac{p^2 {I_X}^2}{4{I_Z}^2 S_g}\alpha = \frac{p^2 {I_X}^2}{4{I_z}^2 S_g}\eta\delta \tag{34}$$

$$\theta = \gamma + \alpha \tag{35}$$

where here we define:

$$\eta = \frac{C_{M_\delta}}{C_{M_\alpha}} \tag{36}$$

Define the distance to the full roll 2π

$$\nu \triangleq \frac{2\pi V}{p} \tag{37}$$

and another characteristic distance;

$$\lambda \triangleq \frac{\nu I_z}{I_x} \tag{38}$$

Let

$$t_\lambda \triangleq \sqrt{\frac{2\lambda}{G_{eff}}} \tag{39}$$

$$\xi = \frac{t}{t_\lambda} \tag{40}$$

Following a similar derivation as in Section 2.1, with a non-dimensional distance variable $s = \xi^2$, and with the same definitions for $\omega = \xi\alpha$ and $\omega_\delta = \xi\delta$ (both complex quantities), we get the LTI equation:

$$\frac{d^2\omega}{ds^2} - 2\pi i\frac{d\omega}{ds} - \frac{\pi^2}{S_g}\omega = \frac{\pi^2}{S_g}\eta\omega_\delta \tag{41}$$

Remark: It is easy to check that the eigenvalues of the homogeneous equation are (recall that $S_g > 1$) :

$$\pi i\left(1 + \sqrt{1 - \frac{1}{S_g}}\right);\ \pi i\left(1 - \sqrt{1 - \frac{1}{S_g}}\right) \tag{42}$$

the two terms correspond to the nutations and precessions of the rocket.

3.2 Control Design

Let $\omega = \omega_Z + i\omega_Y$ and a similar definition for ω_δ. Define a state vector

$$x = \begin{bmatrix} \omega_Z \\ \frac{d\omega_Z}{ds} \\ \omega_Y \\ \frac{d\omega_Y}{ds} \end{bmatrix} \tag{43}$$

and a control vector

$$u = \begin{bmatrix} \omega_{\delta Z} \\ \omega_{\delta Y} \end{bmatrix} \tag{44}$$

Then the state-space matrices A and B of the last equation (41) may be written as:

$$\frac{dx}{ds} = Ax + Bu \tag{45}$$

where

$$A = \begin{bmatrix} 0 & 1 & 0 & 0 \\ \left(\frac{\pi^2}{S_g}\right) & 0 & 0 & -2\pi \\ 0 & 0 & 0 & 1 \\ 0 & 2\pi & \left(\frac{\pi^2}{S_g}\right) & 0 \end{bmatrix} \tag{46}$$

$$B = \eta \begin{bmatrix} 0 & 0 \\ \left(\frac{\pi^2}{S_g}\right) & 0 \\ 0 & 0 \\ 0 & \left(\frac{\pi^2}{S_g}\right) \end{bmatrix} \tag{47}$$

We will examine PD controller based, e.g. on pole placement in the *s* domain. We then obtain in the *time* domain, by the same procedure as in Section IIb, the following feedback law:

$$\delta_Z(t) = (k_{11} + k_{12}\frac{t_\lambda^2}{2t^2})\alpha_Z + k_{12}\frac{t_\lambda^2}{2t}\frac{d\alpha_Z}{dt} + (k_{13} + k_{14}\frac{t_\lambda^2}{2t^2})\alpha_Y + k_{14}\frac{t_\lambda^2}{2t}\frac{d\alpha_Y}{dt} \tag{48}$$

$$\delta_Y(t) = (k_{21} + k_{22}\frac{t_\lambda^2}{2t^2})\alpha_Z + k_{22}\frac{t_\lambda^2}{2t}\frac{d\alpha_Z}{dt} + (k_{23} + k_{24}\frac{t_\lambda^2}{2t^2})\alpha_Y + k_{24}\frac{t_\lambda^2}{2t}\frac{d\alpha_Y}{dt} \tag{49}$$

where the matrix K is obtained from the desired poles for A+BK.

3.3 Representative Example

We consider a hypothetical spinning rocket whose parameters are specified in Tables 2 and 3.

The open-loop eigenvalues of the system (41) are:

$$\{-0.0000 \pm 4.9554i, \quad 0.0000 \pm 1.3278i\}$$

Parameter	Value	Units
m_0	97.4	$[kg]$
m_p	33.9	$[kg]$
I_Z	68.2	$[kg \cdot m^2]$
I_X	1.36	$[kg \cdot m^2]$

Table 2 Mass and inertia parameters.

Parameter	Value	Units
$\dot{p}$	500	$[rad/sec]$
S_g	1.5	[1]
G_{eff}	1000	$[\frac{m}{s^2}]$
ν	12.6	$[m]$
λ	628	$[m]$
t_λ	1.12	$[sec]$
t_b	2	$[sec]$
η	1	[1]

Table 3 Dynamic and flight parameters.

The state feedback gain matrix K was selected as:

$$K = \begin{bmatrix} 4.40 & 1.01 & 0.34 & 4.35 \\ -0.34 & -4.35 & 4.40 & 1.01 \end{bmatrix} \tag{50}$$

With this gain matrix, the resulting closed-loop eigenvalues of *(A-BK)* are:

$$\{-3.6220 \pm 11.6990i, \quad -0.3653 \pm 0.8093i\}$$

Fig. 7 presents the closed loop response to the initial condition in α_Z of Eq. 45 .

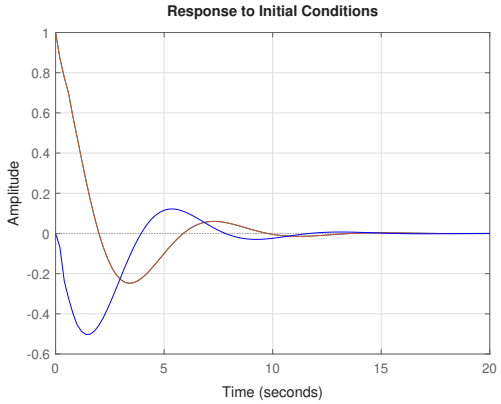

Fig. 7 initial α, red- α_Z , blue- α_Y

Figures 8, 9 and 10 compare the open-loop and closed-loop responses of the *full* system (Equations (33)-(36)) for three scenarios: an initial tip-off rate of 0.5 rad/s, a 50 m/s gust lasting 0.5 seconds, and

a thrust misalignment of 1 mm, respectively. The controls deflections were limited to 0.5 rad. The improved closed-loop performance clearly validates the control design.

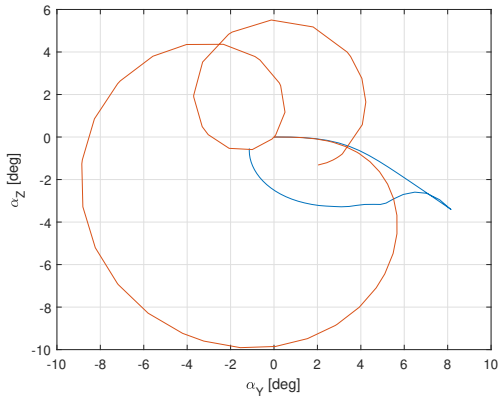

Fig. 8 1^{st} **scenario, tipoff, red- open loop blue- closed loop**

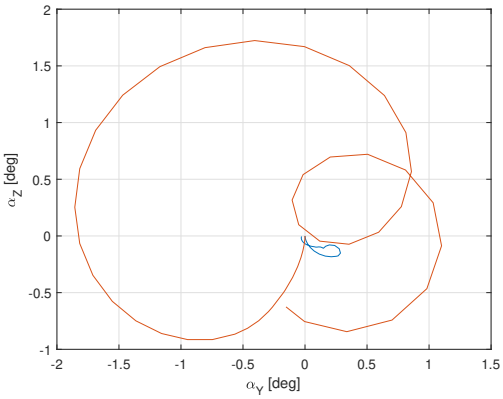

Fig. 9 2^{nd} **scenario, gust, red-open loop blue- closed loop**

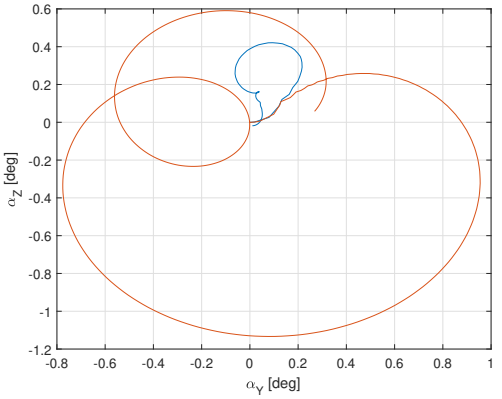

Fig. 10 3^{rd} **scenario, thrust misalignment , red-open loop blue- closed loop**

4 Conclusion

A straightforward method for designing the control of accelerating rockets has been suggested, relying on an approximate time-invariant linear system with distance taken as the independent variable. Simple PD and PID controls have been used for demonstration. Transforming the control laws to time

domain results in *linear time-varying* feedback control laws. While the control designs were developed based on the simplified linear dynamic system, they were verified against a more complete nonlinear dynamics of the rocket. The simplified model ignores specific aerodynamic coefficients, namely C_{L_α} and C_{M_q}, which contribute to damping, rendering it more conservative compared to the full model.

Declaration of Use of Artificial Intelligence

Artificial intelligence was not used in the work presented (other than proofreading).

References

[1] Wozniak J. G. H White D. P. and Lawrence D. A. Missile autopilot design using a gain scheduling technique. In *Proceedings of the 26th Southeastern Symposium on System Theory, Athens OH*, pages 606–610, 1994.

[2] D. A. Lawrence and W. J. Rugh. Gain scheduling dynamic linear controllers for a nonlinear plant. In *Proceedings of the 32nd IEEE Conference on Decision and Control, San-Antonio TX*, pages 1024–1029, 1993.

[3] Mehrabian A. R. and Roshanian J. Design of gain scheduled autopilot for a highly-agile missile. In *Proceedings of the 1st International Symposium on Systems and Control in Aerospace and Astronautics, Harbin, China*, pages 144–149, 2006.

[4] Florian Biertümpfel, Nopporn Pholdee, Samir Bennani, and Hans Pfifer. Finite horizon worst-case analysis of linear time-varying systems applied to launch vehicle. *IEEE Transactions on Control Systems Technology*, 31(6):2393–2404, 2023. doi: 10.1109/TCST.2023.3260213.

[5] Florian Biertümpfel, Hans Pfifer, and Jens Theis. Robust space launcher control with time-varying objectives. *Journal of Guidance, Control, and Dynamics*, 47(4):eG007632, 2024. doi: 10.2514/1.G007632.

[6] J. Gratt and W. L. McCowan. Feedback linearization autopilot design for the advanced kinetic energy missile boost phase. *Journal of Guidance, Control and Dynamics*, 18(5):945–950, 1995.

[7] Ryu S.-M. D.-Y. Won C.-H. Lee and M.-J. Tahk. Missile autopilot design for agile turn control during boost phase. *Int. J. Aeronautical Space Sci.*, 12(4):365–370, 12011.

[8] Y. Lee Y. Kim G. Moon and B.-E. Jun. Sliding mode based attitude and acceleration controller for a velocity-varying skid-to-turn missile. In *Proc. IEEE Eur. Control Conf.,Strasbourg, France*, pages 2951–2956, 2014.

[9] Y. Lee Y. Kim G. Moon and B.-E. Jun. Missile autopilot design during boost phase using robust backstepping approach. In *Proc. AIAA Guid., Navigation, Control Conf., Kissimmee, FL*, pages 1–24, 2015.

[10] Blitzer L. Davis L. Jr., Follin J. W. The exterior ballistics of rockets. *Princeton Toronto London New York, D. Van Nostrand Co., Inc*, 1958. doi: http://dx.doi.org/10.1063/1.3062739.

[11] Mor Friedler and Joseph Z. Ben-Asher. Finding the worst-case behavior of an accelerating rocket due to side-wind disturbances,. *Journal of Spacecraft and Rockets*, 59(5):1787–1794, 2022.